Supporting Information:

Insights into the Importance of WPD-Loop Sequence for Activity and Structure in Protein Tyrosine Phosphatases

Ruidan Shen,[a] Rory M. Crean,[b] Keith J. Olsen,[a] Marina Corbella,[b] Ana R. Calixto,[b] Teisha Richan,[a] Tiago A. S. Brandão,[c] Ryan D. Berry,[a] Alex Tolman,[a] J. Patrick Loria,[d,e] Sean J. Johnson,*[,a] Shina C. L. Kamerlin,*[,b,f] and Alvan C. Hengge*[,a]

[a] Department of Chemistry and Biochemistry, Utah State University, Logan, Utah 84322-0300, USA.

[b] Science for Life Laboratory, Department of Chemistry − BMC, Uppsala University, BMC, Box 576, S-751 23 Uppsala, Sweden.

[c] Departamento de Química, ICEX, Universidade Federal de Minas Gerais, Belo Horizonte, Minas Gerais, 31270-901, Brazil.

[d] Department of Chemistry, Yale University, 225 Prospect Street, New Haven, CT 06520.

[e] Department of Molecular Biophysics and Biochemistry, Yale University, 266 Whitney Avenue, New Haven, CT 06520, USA.

[f] School of Chemistry and Biochemistry, Georgia Institute of Technology, 901 Atlantic Drive NW, Atlanta, GA 30332-0400

Corresponding author email addresses:

Sean J. Johnson: sean.johnson@usu.edu

Alvan C. Hengge: alvan.hengge@usu.edu

Shina C. L. Kamerlin: shina.kamerlin@chemistry.gatech.edu

Table of Contents

Supplementary Methodology

Structure Preparation for Molecular Dynamics Simulations

We have previously[1] prepared structures of wild-type (WT) PTP1B in both conformational states (WPD-loop closed or open) and herein, we used these same starting structures. For the simulations of the Chimeras, where possible we used the available relevant crystal structure, and if one was not available, we modified the most closely related crystal structure (as similar as possible WPD-loop sequence and same WPD-loop conformational state). The structures used for all simulations are provided in **Table S3**. Preparation of the Chimera structures was done using the same process as that we performed for the WT PTP1B structures, meaning all starting structures were subjected to optimization with MolProbity[2] (to perform any required Asn or Gln side chain flips or histidine tautomerization state changes) and PROPKA v. 3.1[3] was used to validate that the protonation states of all titratable residues were consistent between the WT and all chimeras. Consistent with the chemical mechanism of the second step (in which the WPD-loop Asp acts as a base), the catalytic asp was simulated in the deprotonated state. Any missing residues in the remaining scaffold of the chimera structures were added back in using the WT PTP1B structure 6B90[4] as the template. Crystallographic waters were retained for all systems unless a direct clash was observed when the structure was mutated to make the necessary changes for that Chimera (see **Table S3**).

Equilibration and Production Procedures for Molecular Dynamics Simulations

Both the MD equilibration and production procedures used were the same as that we have used previously.[5] A total of 50 μs of Production MD simulations were run for each system in order to

generate Markov state models (MSMs) describing WPD-loop and E-loop motion (described in the main text **Materials and Methods**).

In order to equilibrate each system the following protocol was used: Hydrogens atoms and solvent molecules were energy minimized (using 500 steps of steepest descent followed by 500 steps of conjugate gradient minimization). To prevent the movement of non-hydrogen and non-solvent atoms during the minimization, 10 kcal mol^{-1} $Å^{-1}$ positional restraints were used to keep all (non-solvent) heavy atoms fixed. The solvent was then heated rapidly from 50 K to 298 K (NVT ensemble, 1 fs timestep) over the course of 200 ps, with the previously described restraints still maintained. These positional restraints were then replaced with 5 kcal mol^{-1} $Å^{-1}$ positional restraints on only the C_α carbon atoms of each residue and subjected to another round of energy minimization (500 steps of steepest descent followed by 500 steps of conjugate gradient). Retaining these positional restraints, the system was heated from 25 K to 298 K over the course of 50 ps (NVT ensemble, 1 fs time step). Simulations were then performed in the NPT ensemble (1 atm, 298 K, 2 fs time step) by first gradually reducing the 5 kcal mol^{-1} $Å^{-1}$ C_α carbon restraints over the course of 50 ps. This was done by reducing the restraint weight by 1 kcal mol^{-1} $Å^{-1}$ every 10 ps. A final 1 ns long NVT MD simulation with no restraints placed on the system was then performed, with the final structure produced after this run, used as the starting point for production MD simulations.

Production MD simulations were run with a 2 fs time step (with the SHAKE[6] algorithm applied) and an 8 Å direct space non-bonded cut-off, with long range electrostatics evaluated using the particle-mesh Ewald[7] method. Temperature and pressure were regulated using Langevin temperature control (collision frequency of 1 ps^{-1}) and a Berendsen barostat (pressure relaxation time of 1 ps).

Supplementary Figures

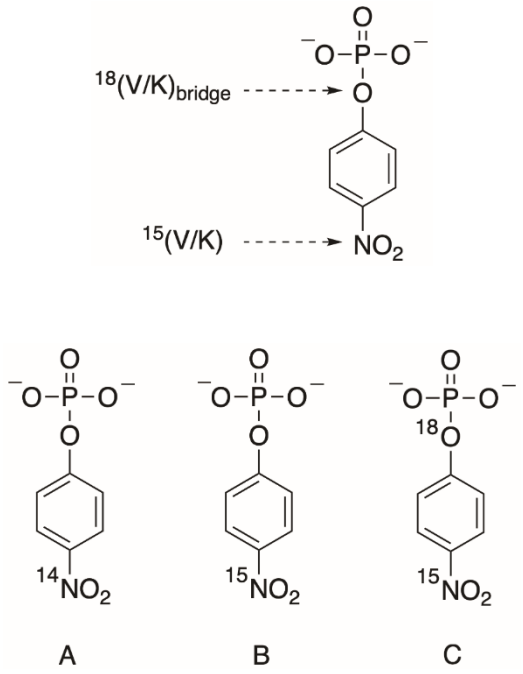

Figure S1. Top, the substrate *p*-nitrophenyl phosphate (*p*NPP) showing the positions where kinetic isotope effects were measured: the bridge oxygen atom, the position of bond cleavage, $^{18}(V/K)_{bridge}$, and the nitrogen atom in the leaving group, $^{15}(V/K)$. Below, the isotopic isomers used for KIE measurements. Natural abundance *p*NPP consists of a mixture of A and B and was used for measurement of $^{15}(V/K)$. The isotopic isomers A and C were synthesized as described in the manuscript and mixed to prepare the substrate used for measuring the bridging-$^{18}(V/K)_{bridge}$.

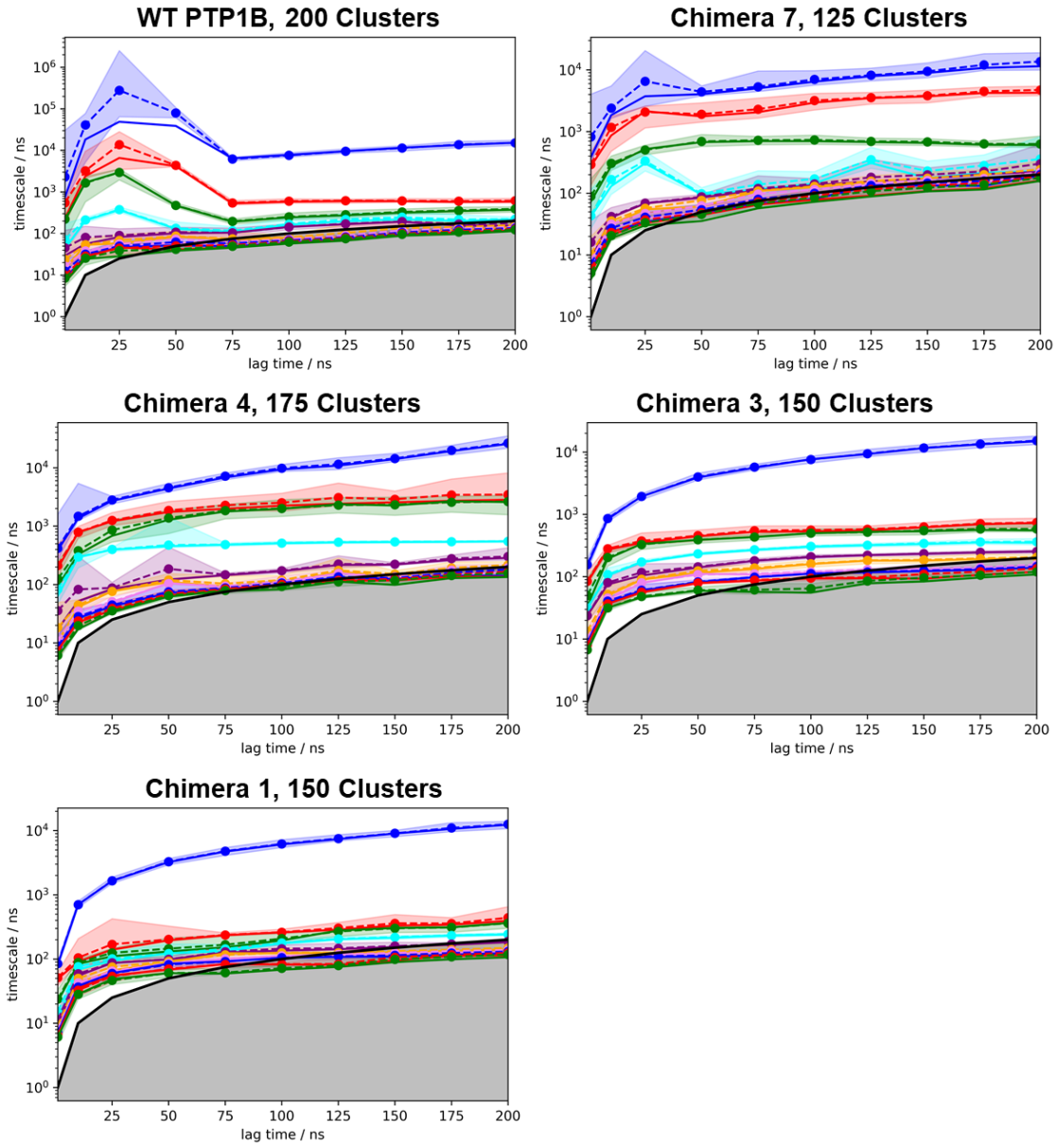

Figure S2. Implied timescales estimated at a range of lag times for WT PTP1B and each Chimera simulated. The shaded region of each line plot depicts the 95% confidence intervals by a Bayesian MSM. This data was used to select an appropriate lag time to build the Markov state models. The number of clusters used to discretise the datasets prior to the implied timescale calculation is given. See the **Materials and Methods** for further information.

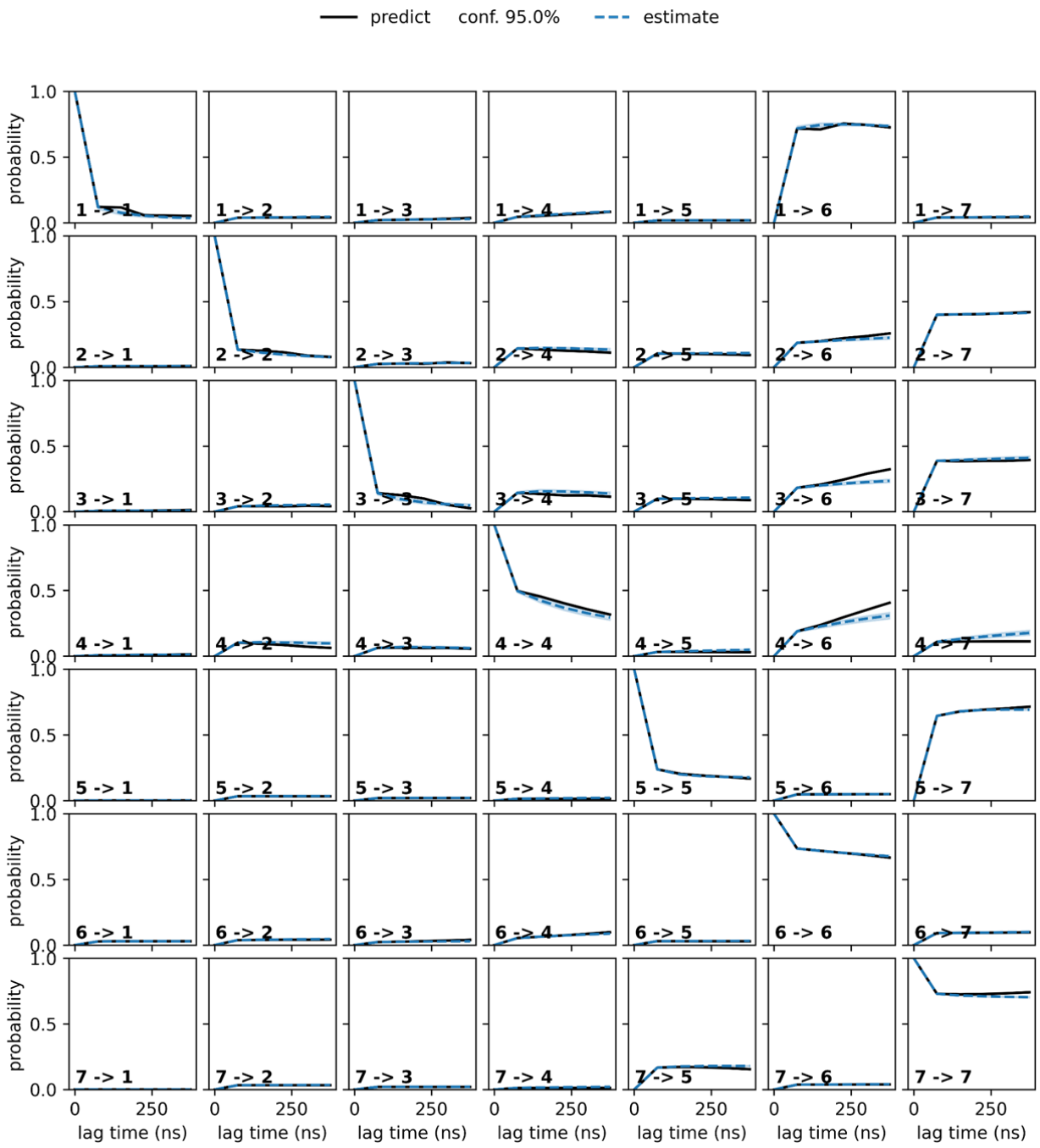

Figure S3. Chapman-Kolmogorov test for the Markovianity of the constructed MSM for simulations of WT PTP1B, using a lag time of 75 ns. These show the probabilities of transitioning between every macrostate to every other macrostate.

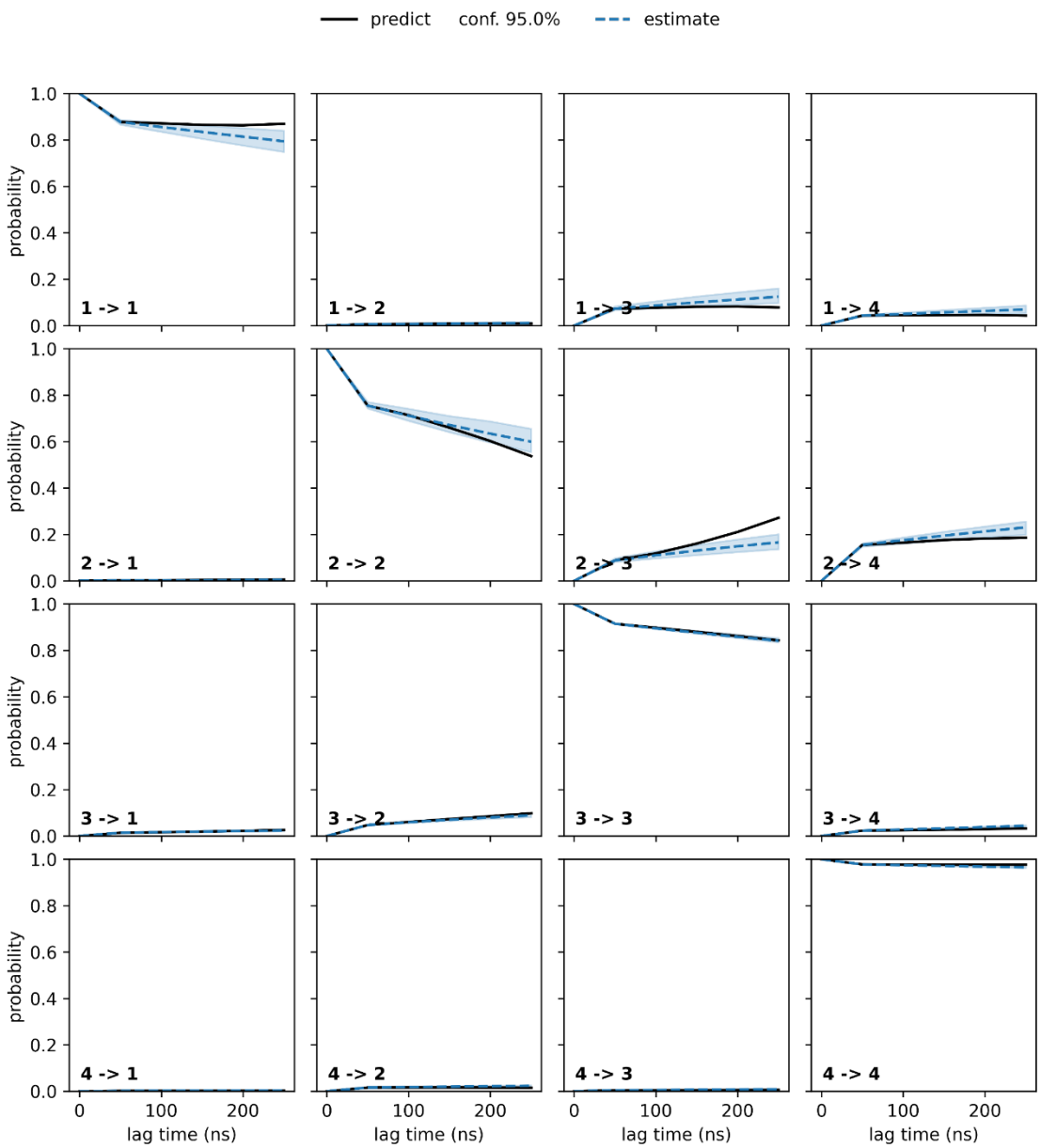

Figure S4. Chapman-Kolmogorov test for the Markovianity of the constructed MSM for simulations of Chimera 7, using a lag time of 75 ns. These show the probabilities of transitioning between every macrostate to every other macrostate.

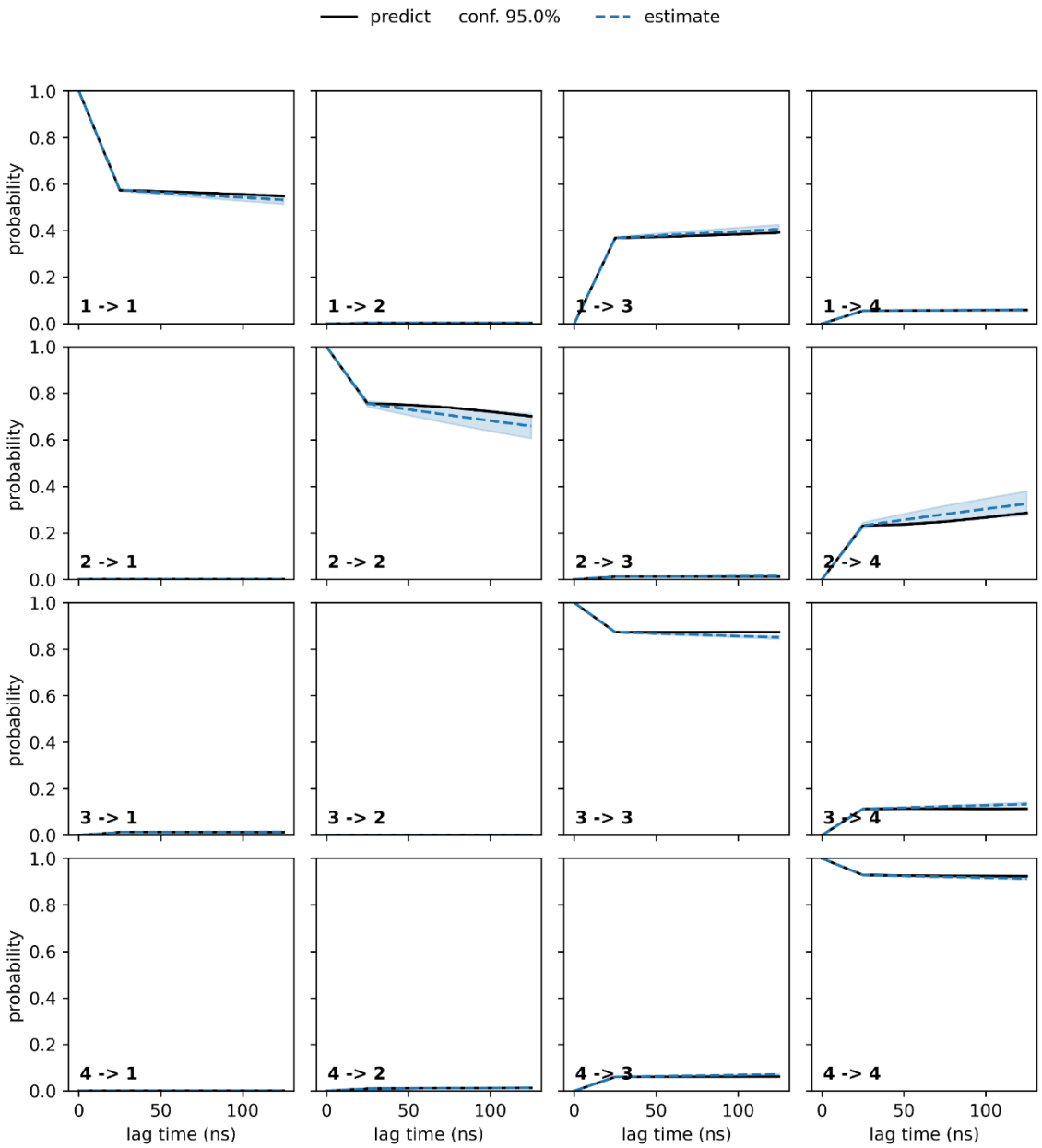

Figure S5. Chapman-Kolmogorov test for the Markovianity of the constructed MSM for simulations of Chimera 4, using a lag time of 75 ns. These show the probabilities of transitioning between every macrostate to every other macrostate.

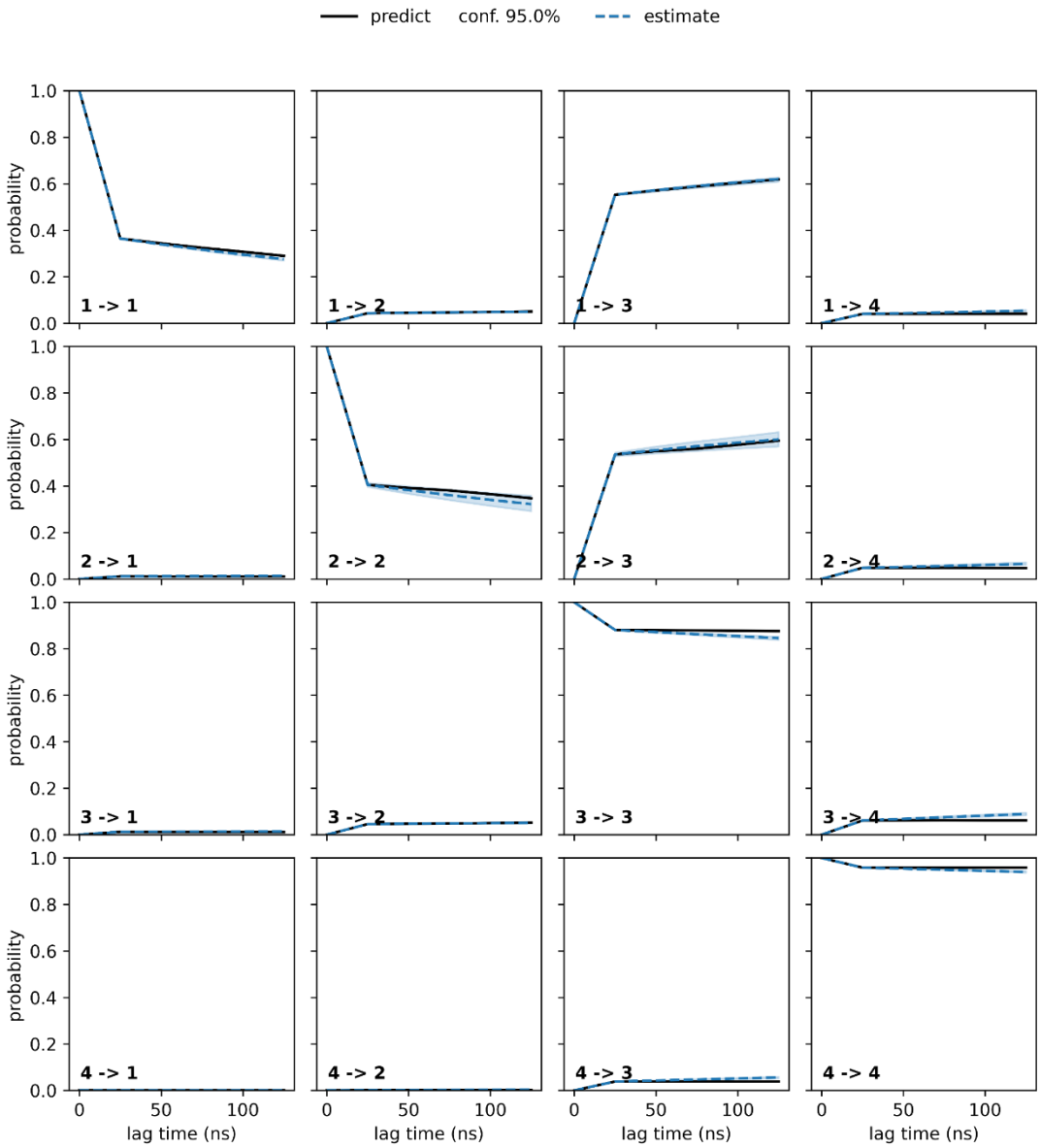

Figure S6. Chapman-Kolmogorov test for the Markovianity of the constructed MSM for simulations of Chimera 3, using a lag time of 75 ns. These show the probabilities of transitioning between every macrostate to every other macrostate.

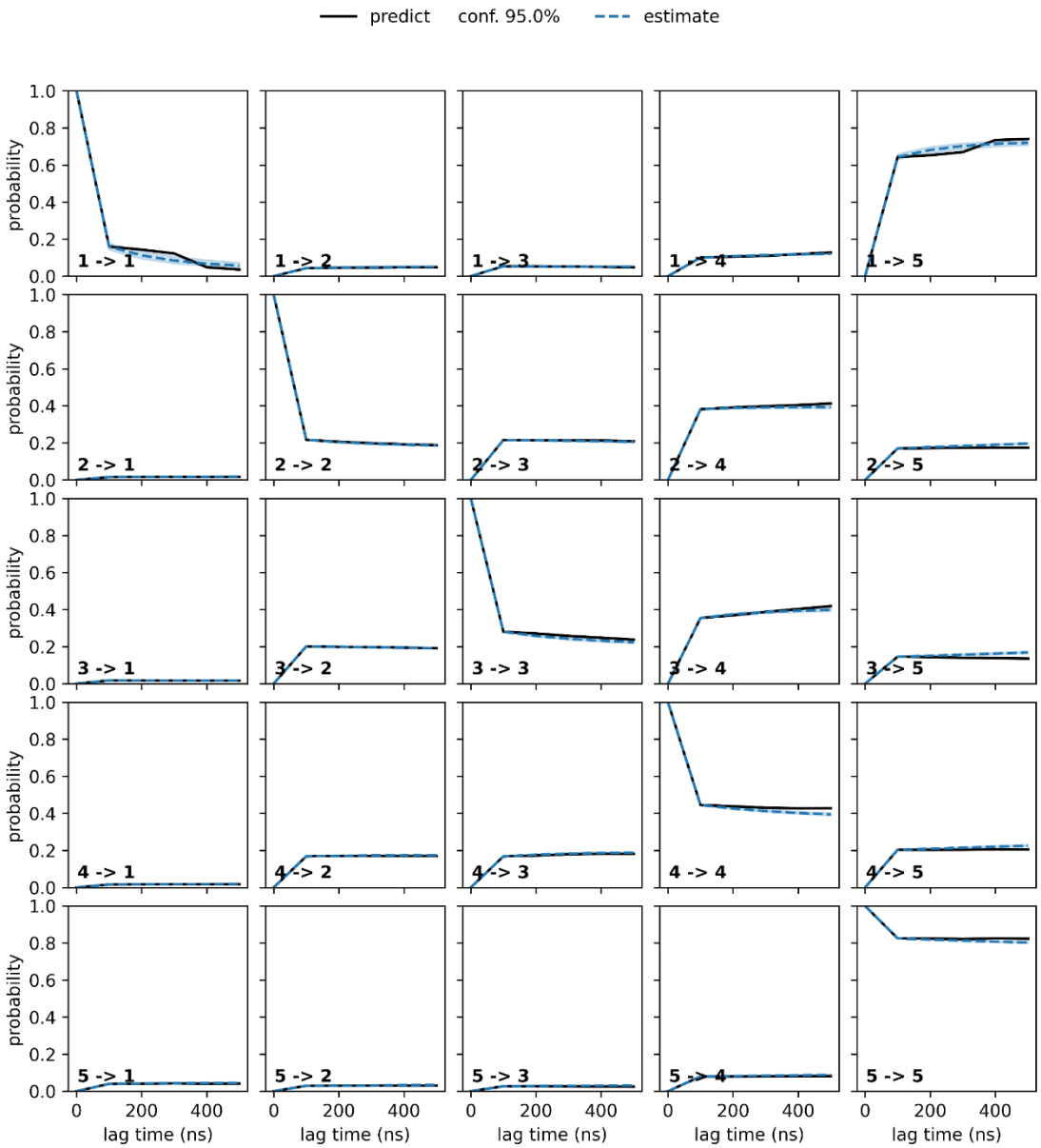

Figure S7. Chapman-Kolmogorov test for the Markovianity of the constructed MSM for simulations of Chimera 1, using a lag time of 75 ns. These show the probabilities of transitioning between every macrostate to every other macrostate.

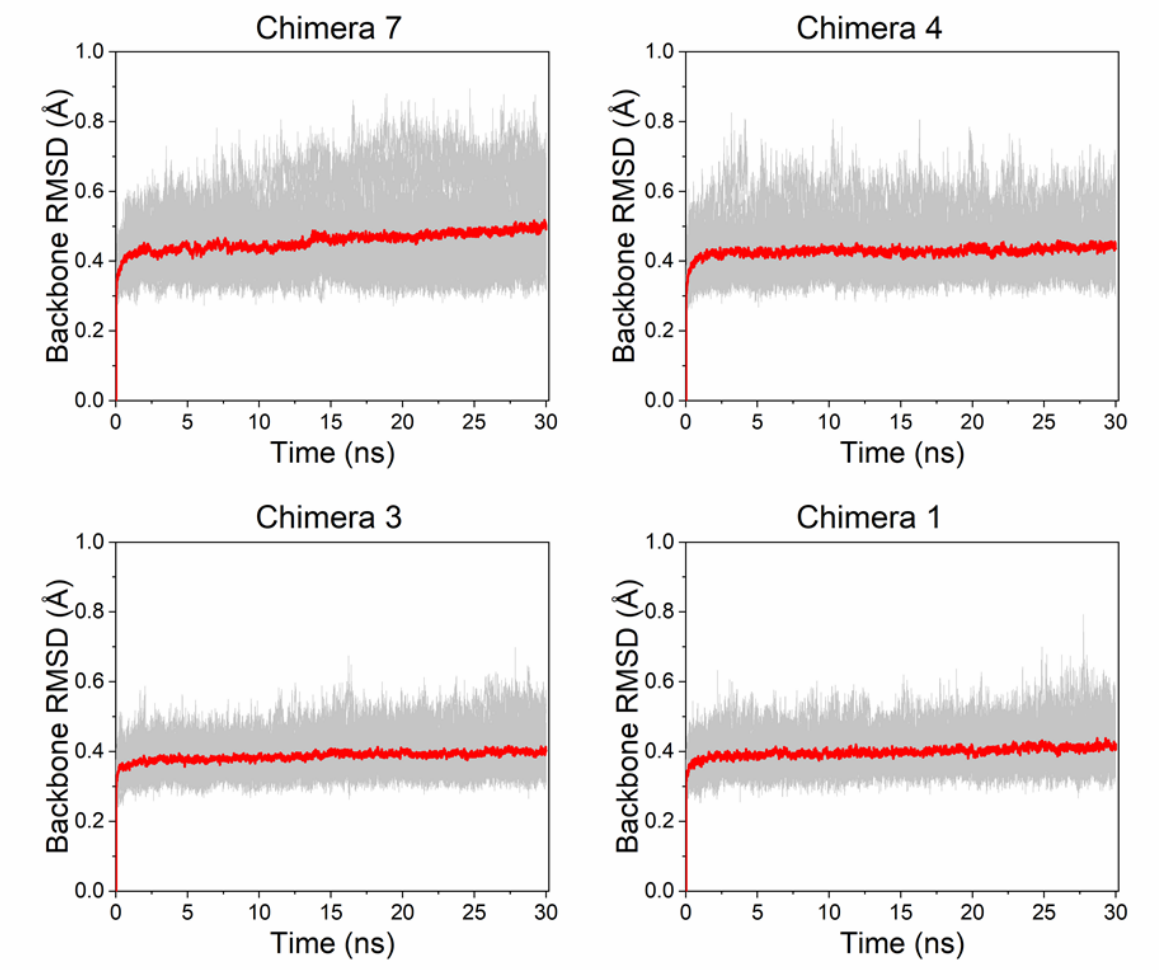

Figure S8. The root mean square deviations (RMSD, Å) of all backbone atoms during our EVB equilibration MD simulations. Equilibration simulations were performed at the approximate EVB transition states ($\lambda = 0.5$) for all PTPs in the second catalytic step (hydrolysis). Data was collected every 10 ps from 30 replicas each of length 30 ns. The grey lines show the 30 individual runs, whilst the red line shows a rolling average RMSD from all 30 replicas.

Figure S9. Overview of the sequence variability of the WPD-loop of classical PTPs (as defined by Chen *et al*.[8]), as well as the canonical YopH sequence. This figure was originally presented in ref. [5]. For details of how the alignment was generated, see the caption to **Figure S1** of ref. [5].

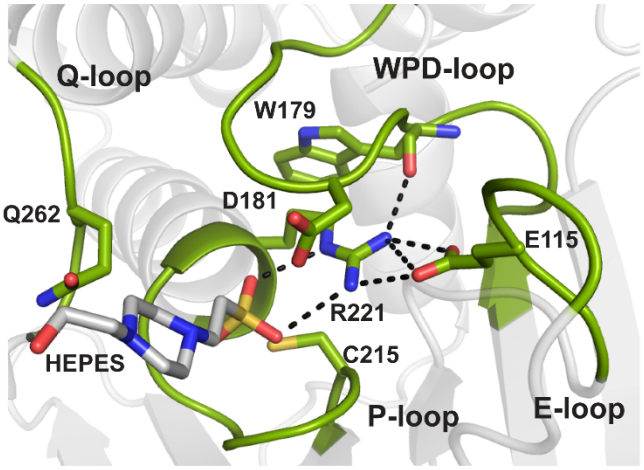

Figure S10. Polar interactions at the active site in the crystal structure of Chimera 7 with bound HEPES. Catalytic residues and their polar neighbors are shown in sticks. The three sulfonyl oxygen atoms of HEPES hydrogen bond to NH amides in the main chain of the P-loop and also to the Arg221 side chain. The WPD-loop is in the closed conformation and the Arg221 side chain is hydrogen-bonded to Trp179 carbonyl oxygen, the same orientation observed in the WT PTP1B loop-closed conformation. The substituted residue Gln182 is oriented on the top of the active site and hydrogen bonds to water molecule W1, which also coordinates to an oxygen atom of Hepes, the side chain of Gln266, and the backbone amide proton of Gln182. This water molecule is common to other X-ray structures in the catalytic pathway of PTP1B wildtype and is also observed in other members of the PTP family (*e.g*. *Yersinia* PTP and PTPβ).[9, 10] HEPES is commonly used as a buffer in the crystallization of PTP1B. It is a poor competitive inhibitor of PTPs and binding at the active site is not commonly observed in X-ray structures. The alkyl ring of HEPES is oriented in a position that could clash with the side chain of F182 in the native enzyme, so the F182Q mutation likely allows HEPES binding.

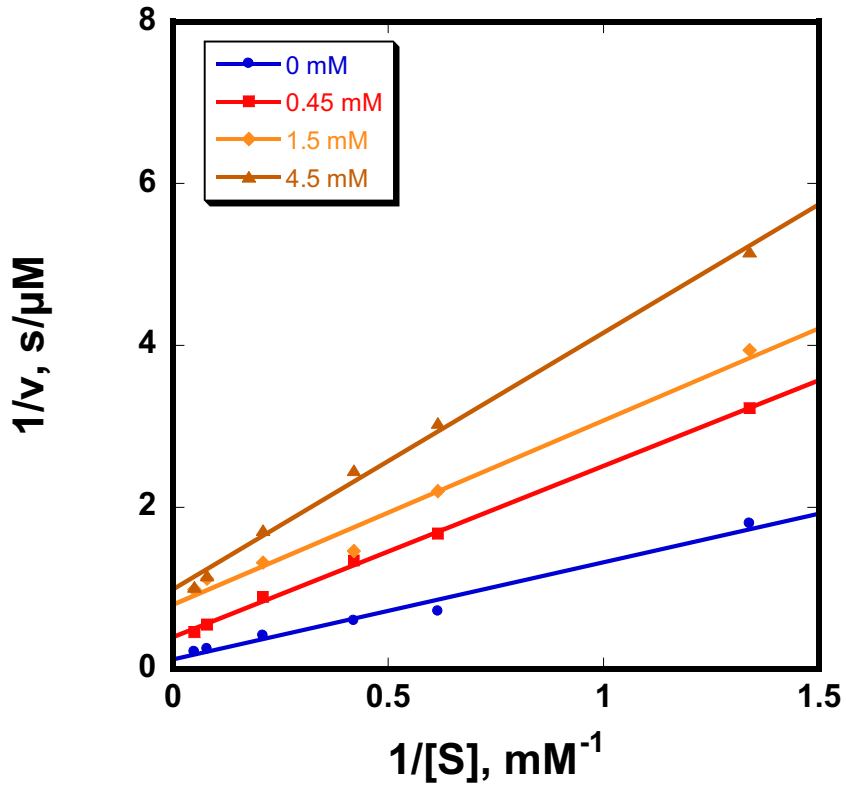

Figure S11. Magnesium shows inhibitory effects on Chimera 4. Magnesium concentrations are given in the inset.

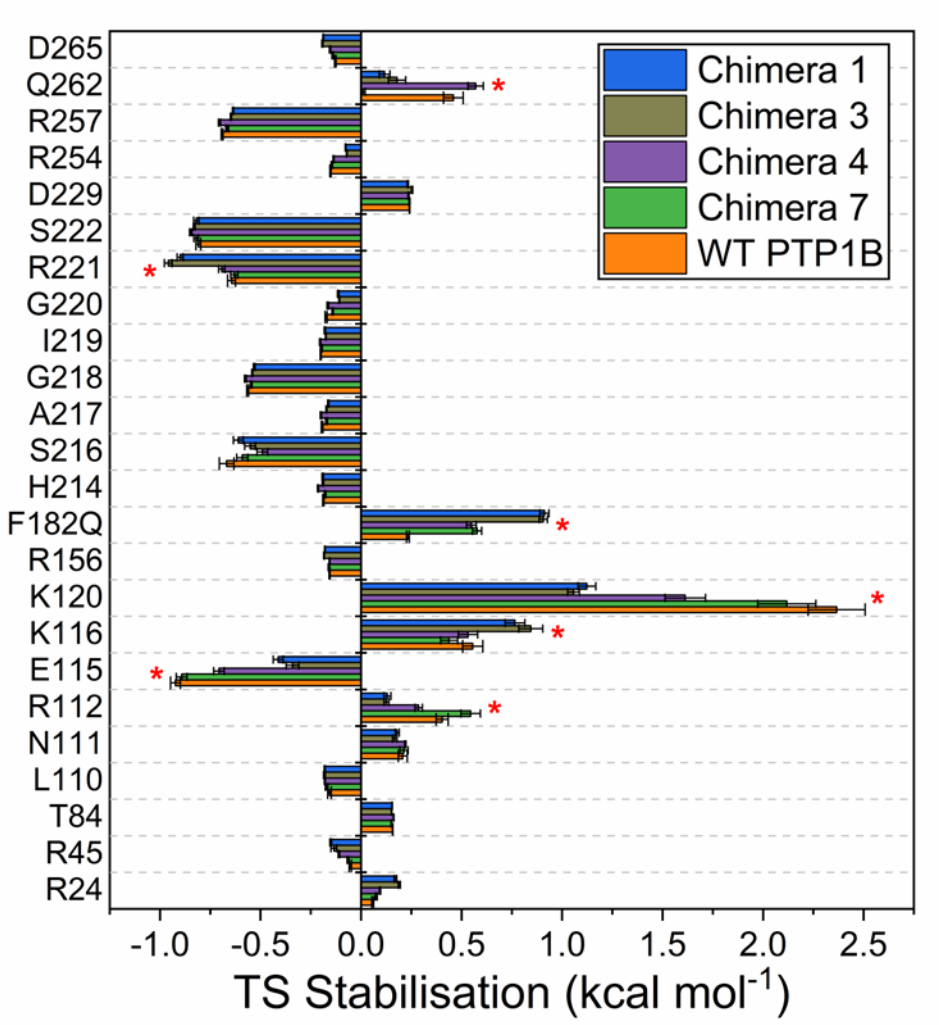

Figure S12. Electrostatic contributions of individual amino acids ($\Delta\Delta G^{\ddagger}_{elec}$, kcal mol^{-1}) to the calculated activation free energies for the hydrolysis reaction catalyzed by WT PTP1B and relevant chimeras. The seven residues depicted in **Figure 5B** are indicated with a red asterix and were selected because in at least one Chimera the difference in electrostatic contributions (relative to the WT) was $\geqslant |0.25|$ kcal mol^{-1}. This data is provided in tabular form in **Table S8**.

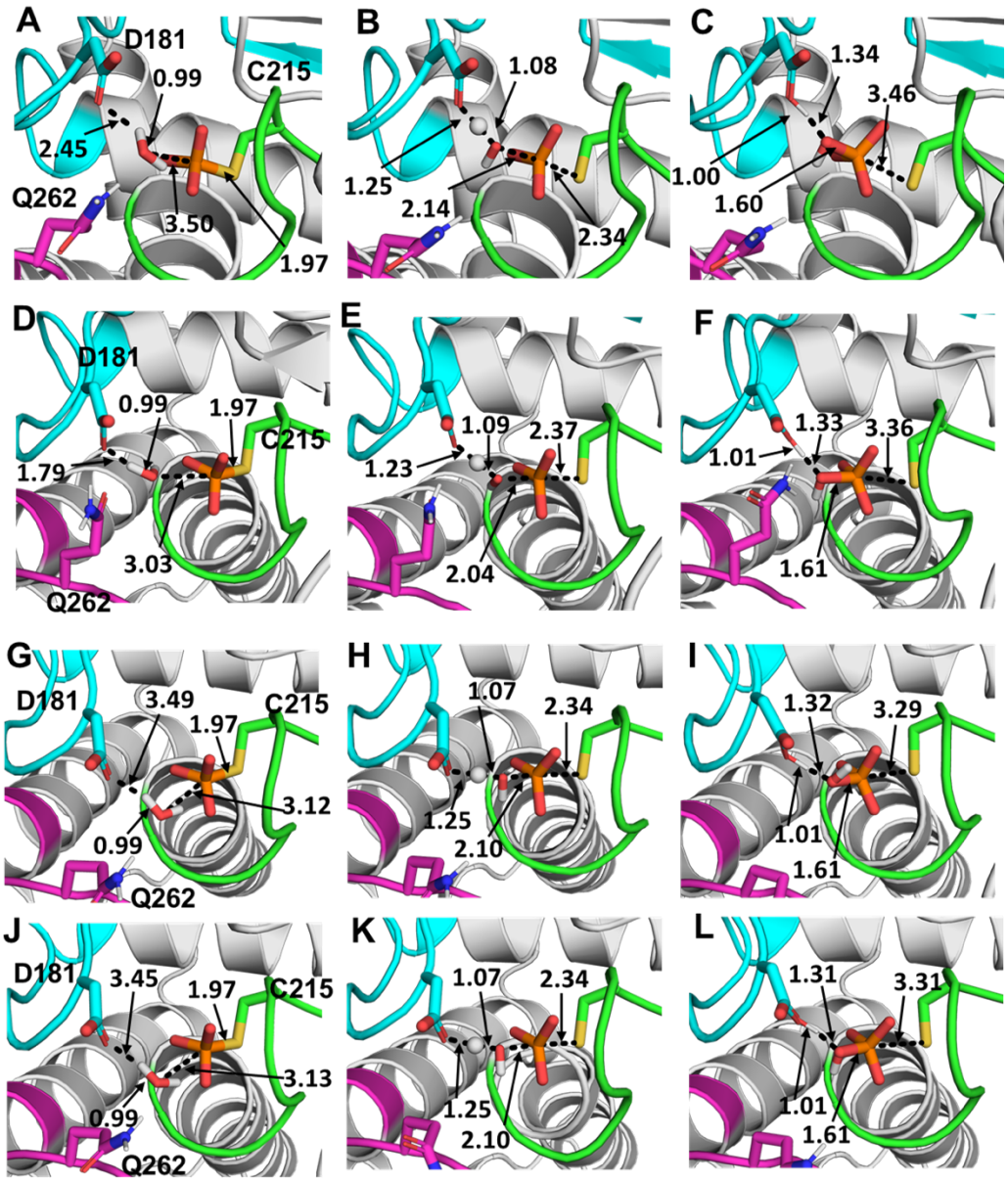

Figure S13. Representative structures of (**A**, **D**, **G**, **J**) the phosphoenzyme intermediate, (**B**, **E**, **H**, **K**) the transition state for the hydrolysis step, and (**C**, **F**, **I**, **L**) the final product complex for the PTP-catalyzed hydrolysis of *p*NPP of each chimera simulated. Shown here are structures from simulations of (**A**-**C**) Chimera 7, (**D**-**F**) Chimera 4, (**I**-**K**) Chimera 3 and (**J**-**L**) Chimera 1. The structures shown here are the centroids of the top-ranked cluster obtained from RMSD clustering of 30 individual EVB trajectories of each stationary or saddle point. Average reacting distances for each stationary point for each system are shown in **Table S9**.

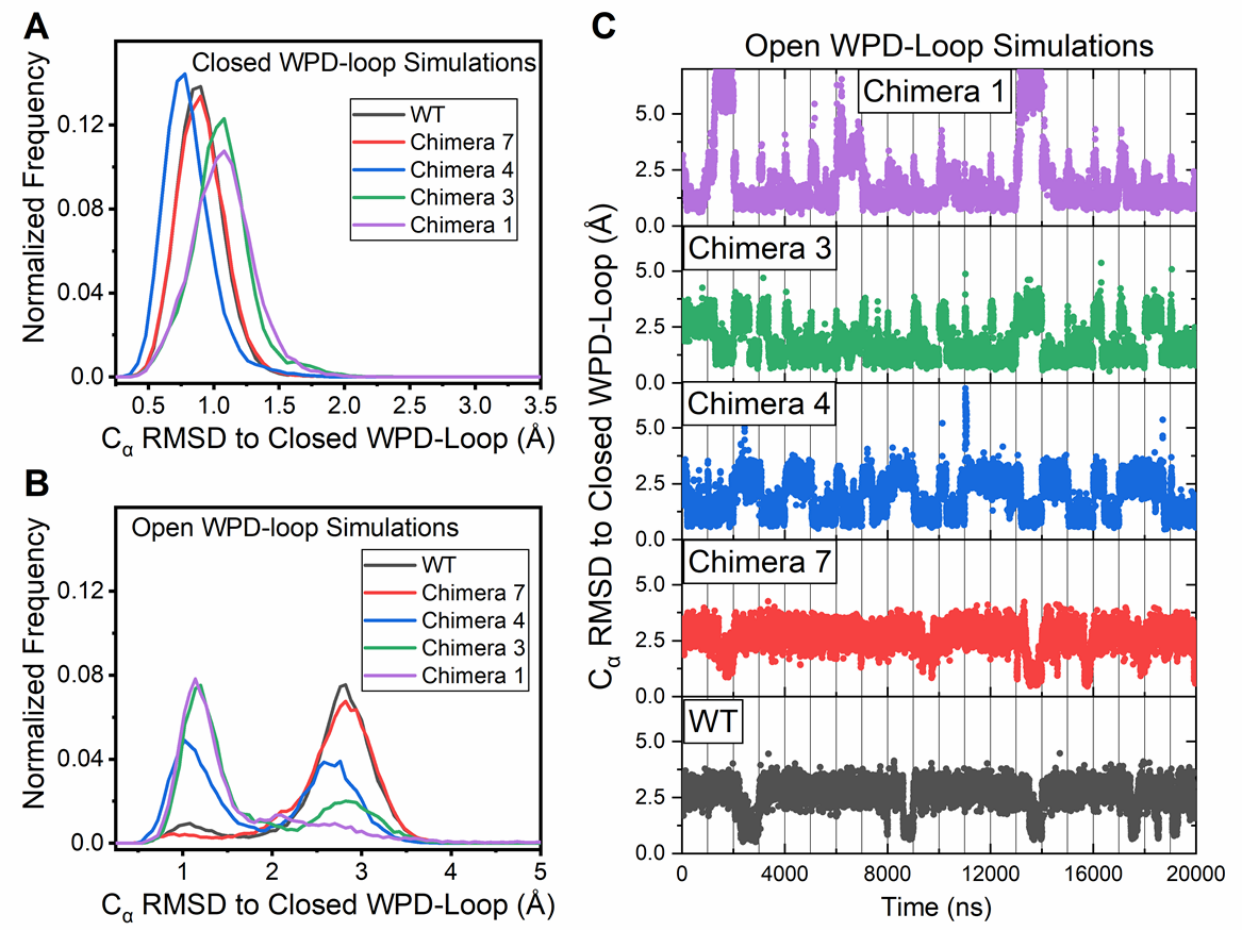

Figure S14. (**A**, **B**) Histograms of the WPD-loop C_α-RMSD for simulations of the WT PTP1B and all 4 chimeras studied, starting from either from the (**A**) closed or (**B**) open WPD-loop conformation (RMSD is measured to the relevant starting crystal structure). (**C**) Plots of the WPD-loop C_α-RMSD for simulations starting from the open WPD-loop conformation, with the reference structure used the closed WPD-loop (a low RMSD value would therefore indicate a transition to the closed WPD-loop conformation). The thin vertical lines along each plot indicate the start/end of an individual replica (20 x 1 μs long replicas were performed per complex).

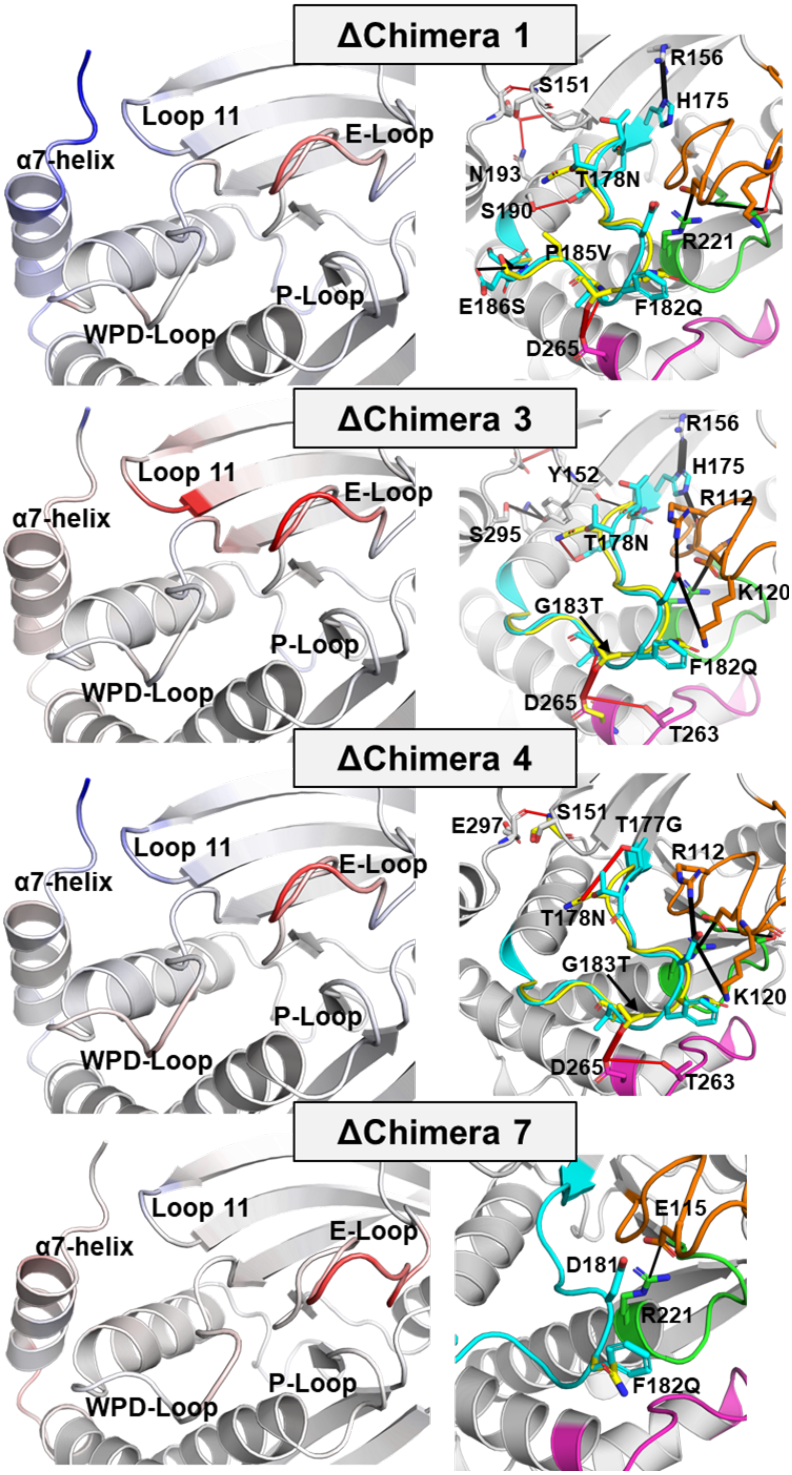

Figure S15. (**Left Panels**) Color mapping of the differences (WT – Chimera) in the calculated per residue C_α RMSF (ΔRMSF) for the simulations of the open WPD-loop. Color mapping was performed from blue (positive ΔRMSF) through to white (0 ΔRMSF value) to red (negative

ΔRMSF). In practice, a blue residue would mean increased rigidity for the given Chimera variant over WT PTP1B and vice versa. (**Right Panels**) Differences in the hydrogen bonding network between WT PTP1B and each Chimera during simulations of each system in a open WPD-loop conformation. Hydrogen bonds with a higher occupancy in the WT are shown as black cylinders between the donor and acceptor atoms, with red cylinders used to indicate H-bonding interactions which have a higher occupancy in a given Chimera. The width of the dash indicates the magnitude of the difference in the occupancy of the hydrogen bond between the two enzymes. The P-, Q- and E-loops are colored green, magenta and orange respectively, with the WT PTP1B WPD-loop colored cyan and Chimera WPD-loop colored yellow.

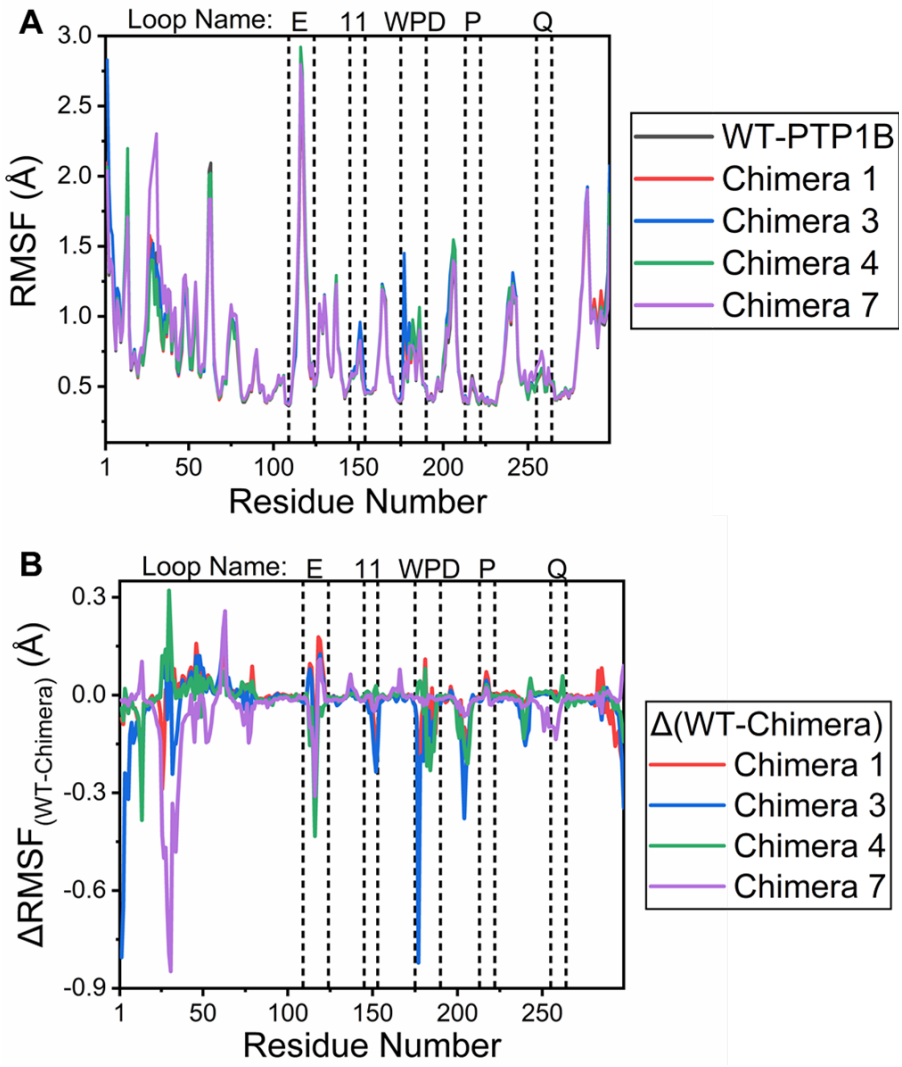

Figure S16. (**A**) Calculated per residue C_α root mean squared fluctuations (RMSF) and (**B**) differences in the per residue C_α RMSF (ΔRMSF) for the closed state of the WT PTP1B to each chimera simulated in this work during our conventional MD simulations. For panel **B**, a negative value would indicate increased flexibility in the Chimera over the WT. Closed state conformations were identified from our MD simulations as structures with a WPD-loop C_α RMSD ≤ 1.5 Å from the closed WPD-loop crystal structure (or starting structure in the case of Chimera 1, see the **Materials and Methods**).

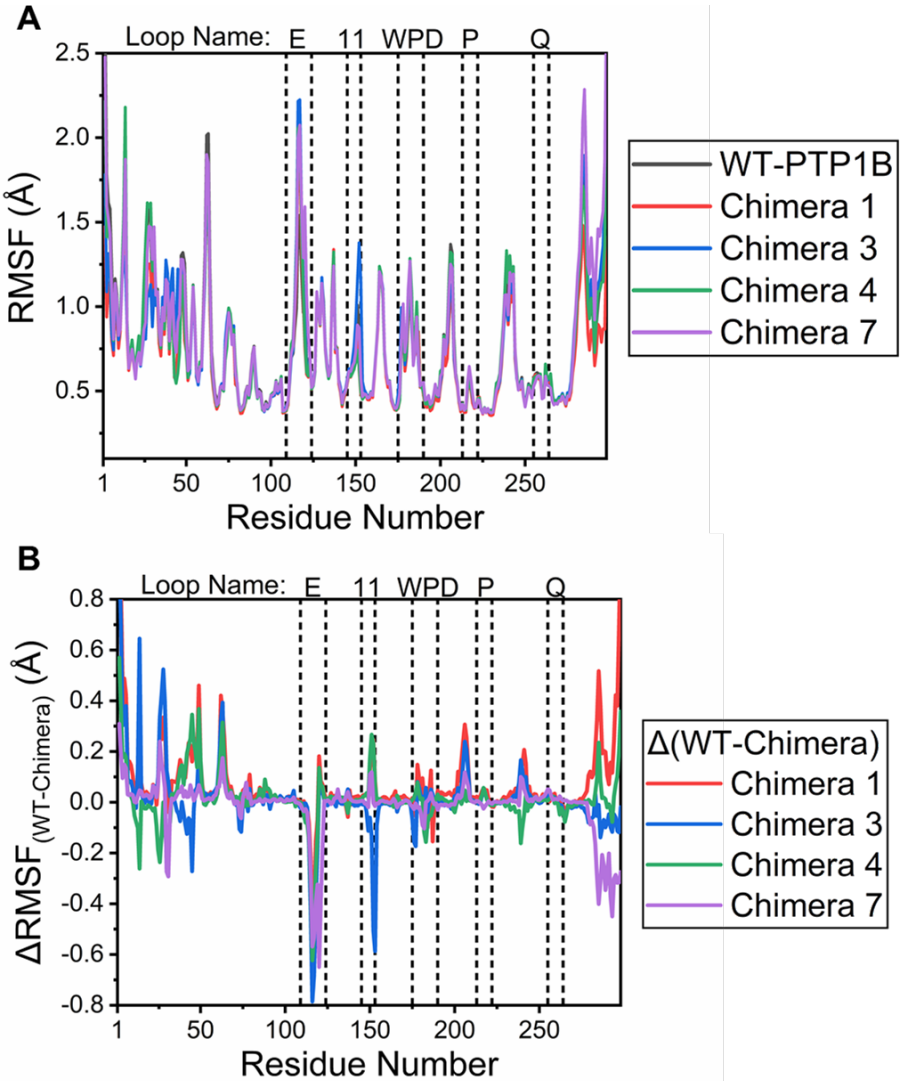

Figure S17. (**A**) Calculated per residue C_α root mean squared fluctuations (RMSF) and (**B**) differences in the per residue C_α RMSF (ΔRMSF) for the open state of the WT PTP1B to each chimera simulated in this work during our conventional MD simulations. For panel **B**, a negative value would indicate increased flexibility in the Chimera over the WT. Open state conformations were identified from our MD simulations as structures with a WPD-loop C_α RMSD ≤ 1.5 Å from the open WPD-loop crystal structure (or starting structure in the case of Chimeras 1 and 3, see the **Materials and Methods**).

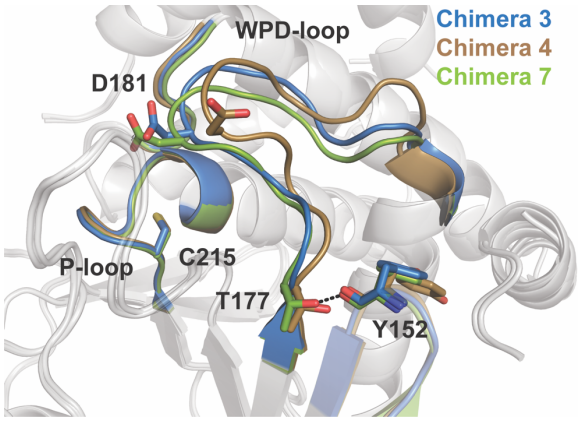

Figure S18. Thr177 in the crystal structure of Chimera 4 affects loop position without perturbing secondary structures at the active site *via* contribution of a hydrogen bond with the backbone carbonyl group of Y152.

Supplementary Tables

Table S1. List of forward and reverse primers used to construct the different PTP1B chimeras studied in this work. Chimera 7 was made using WT PTP1B as a template.

	Forward primer (5'->3')	**Reverse primer (5'->3')**
Chimera 0	GATCAGACCGCAGTCAGCTCACCAGCCTCATTCTTG	GGGCCAATTGCCAACATGGAAATGTAAGATCTCTCGAG
Chimera 1	ACATTTCCATTATGGCAATTGGCCCGATC	GATCGGGCCAATTGCCATAATGGAAATGT
Chimera 3	GCCCGATCAGACCGCAGTCGAGTCACCAGCCTCATTCTTG	CAAGAATGAGGCTGGTGACTCGACTGCGGTCTGATCGGGC
Chimera 4	ATTGGCCCGATCAGACCGCACCCGAGTCACCAGCCTCATTCTT	AAGAATGAGGCTGGTGACTCGGGTGCGGTCTGATCGGGCCAAT
Chimera 7	CCACATGGCCTGACCAGGGAGTCCCTGAATCACC	CCACTAAGTCCCTGAGGGACCAGTCCGGTACACC

Table S2. Data collection and refinement statistics. Values in parentheses are for the highest-resolution shell. CC1/2 values are for the highest-resolution shell.

	Chimera 3 Ligand-	**Chimera 3 WO_4**	**Chimera 3 VO_4**
PBD ID	**6XE8**	**6XED**	**6XEA**
Data Collection			
Source	SSRL 9-1	SSRL 9-1	SSRL 9-1
Space group	$P3_121$	$P3_121$	$P3_121$
Cell dimensions			
a, b, c (Å)	87.96, 87.96,	88.87, 88.87,	88.59, 88.59,
α, β, γ (°)	90, 90, 120	90, 90, 120	90, 90, 120
Resolution (Å)	50.0-1.95 (2.02-	50.0-1.80 (1.86-	50.0-1.55 (1.60-
CC1/2	0.815	0.87	0.726
I / σI	47.9 (2.87)	24.88 (5.00)	35.1 (2.42)
Completeness	99.8 (97.8)	100.0 (99.9)	97.6 (94.4)
Redundancy	17.9 (11.2)	16.4 (9.8)	18.1 (11.6)
No. reflections	33,776 (3,231)	44,952 (4,430)	67,840 (6,493)
Refinement			
R_{work} / R_{free}	0.163/0.185	0.157/0.179	0.187/0.199
No. Atoms			
Protein	2400	2418	2440
Ligand/ion	19	35	23
Water	142	290	213
β-factors			
Protein	49.6	31.2	31.8
Ligand/ion	59.3	35.8	32.9
Solvent	51.6	43.6	39.4
R.m.s			
Bond lengths	0.006	0.006	0.006
Bond angles	0.87	0.84	1.16
Ramachandran			
Favored (%)	97.6	97.6	97.6
Allowed (%)	2.1	2.1	2
Outliers (%)	0.3	0.3	0.3

	Chimera 4 Ligand-	**Chimera 4 WO_4**	**Chimera 4 VO_4**	**Chimera 7 HEPES**
PBD ID	**6XEE**	**6XEG**	**6XEF**	**7S4F**
Data Collection				
Source	SSRL 9-1	SSRL 9-1	SSRL 9-1	Home source
Space group	$P3_121$	$P3_121$	$P3_121$	$P3_121$

Cell dimensions				
a, b, c (Å)	88.40, 88.40,	88.64, 88.64,	88.38, 88.38,	88.3, 88.3, 103.9
α, β, γ (°)	90, 90, 120	90, 90, 120	90, 90, 120	90, 90, 120
Resolution (Å)	50.0-2.50 (2.59-	50.0-2.55 (2.64-	50.0-2.05 (2.12-	22.89-1.65 (1.71-
CC1/2	0.773	0.664	0.576	0.701
I / σI	19.4 (3.0)	16.4 (1.63)	20.9 (1.63)	28.8 (2.1)
Completeness	97.7 (95.6)	99.6 (96.7)	99.8 (98.5)	94.8 (67.3)
Redundancy	16.0 (7.2)	16.2 (5.0)	16.4 (8.2)	5.2 (3.0)
No. reflections	16,320 (1,566)	15,928 (1,510)	30,280 (2,914)	282,736 (53,917)
Refinement				
R_{work} / R_{free}	0.173/0.215	0.161/0.207	0.181/0.203	0.180/0.203
No. Atoms				
Protein	2362	2417	2437	2449
Ligand/ion	33	23	24	28
Water	87	89	137	315
β-factors				
Protein	57.3	47.2	49.3	31.9
Ligand/ion	73.8	55.7	58.8	48.5
Solvent	51	44.2	51.9	42.9
R.m.s				
Bond lengths	0.007	0.008	0.008	0.006
Bond angles	0.88	0.98	1.11	1.03
Ramachandran				
Favored (%)	96.2	95.6	98	98.3
Allowed (%)	3.5	4.1	1.7	1.4
Outliers (%)	0.4	0.3	0.3	0.3

Table S3. All X-ray crystal structures used for our MD simulations of PTP1B and YopH in their unliganded forms.

PTP and WPD-loop conformation	Crystal Structure Used	Modifications/Mutations Required
WT PTP1B		
Closed WPD-loop	6B90[a, 4]	None required.
Open WPD-loop	6B90[a, 4]	None required.
Chimera 1		
Closed WPD-loop	6XED[b]	Mutagenesis of WPD-loop from Chimera 3 sequence to Chimera 1.
Open WPD-loop	6XEE[b]	Mutagenesis of WPD-loop from Chimera 4 sequence to Chimera 1.
Chimera 3		
Closed WPD-loop	6XED[b]	None required.
Open WPD-loop	6XEE[b]	Mutagenesis of WPD-loop from Chimera 4 sequence to Chimera 3.
Chimera 4		
Closed WPD-loop	6XEF[b]	None required.
Open WPD-loop	6XEE[b]	None required.
Chimera 7		
Closed WPD-loop	3QKN[b]	None required.
Open WPD-loop	6B90[a, 4]	F182Q mutation made *in silico*.

[a] Structure contains both closed and open conformations of the WPD-loop. [b] Structures used were generated from this study.

Table S4. Parameters used to build the Markov state models (MSMs) of WT PTP1B and each simulated chimera.[a]

Enzyme	Number of Clusters[b]	Lag Time (ns)[c]	Number of States[d]
PTP1B WT	200	75	7
Chimera 1	150	100	5
Chimera 3	150	25	4
Chimera 4	175	25	4
Chimera 7	125	50	4

[a] The application of each of these parameters to each system is described in the **Materials and Methods**. [b] Number of clusters requested from the *k*-means clustering algorithm. [c] Lag-time chosen to describe the MD simulation length. [d] Number of metastable states selected to build the MSM with.

Table S5. Ionized residues and histidine protonation patterns used in our EVB simulations of Chimeras 1, 3, 4 and 7.

Residue Type	Residue Number
Asp	48, 181, 229, 265
Glu	115, 186[a]
Lys	24, 45, 47, 112, 156, 221, 254, 257
Arg	36, 116, 120
His-ε	25, 54, 60, 94, 173, 175, 208, 296
His-δ	214

[a] Glu186 is Ser186 in Chimera 1. All other residues were kept in their neutral forms as they fell outside of the explicit simulation sphere used in the surface constrained all-atom solvent (SCAAS) model,[11] as described in our prior work.[1]

Table S6. Kinetic pK_a values for wild-type PTP1B, YopH, and Chimeras.[a]

Enzyme	**pK_{a1}**	**pK_{a2}**	**Reference**
PTP1B WT	5.12 ± 0.07	6.36 ± 0.07	[12]
YopH WT	4.6 ± 0.07	5.2 ± 0.06	[13]
Chimera 3	5.0 ± 0.2	7.2 ± 0.1	This work.
Chimera 4	5.2 ± 0.4	5.7 ± 0.4	This work.
Chimera 7	4.5 ± 0.2	6.9 ± 0.2	This work.

[a] Data obtained from fits of the pH-rate profiles shown in **Figure 3** to **Eq. 1**.

Table S7. Calculated activation and reaction free energies, as well as the corresponding experimental values, from EVB simulations of PTP1B, YopH, and relevant chimeras.[a]

	$\Delta G^{\ddagger}_{calc}$	$\Delta G_{0,calc}$	Experimental data			
			k (s^{-1})	Temp (°C)	pH	$\Delta G^{\ddagger}_{exp}$
Hydrolysis						
PTP1B WT	14.3 ± 0.2	-1.4 ± 0.4	28[14]	3.5	5.4	14.3
			48[15-17]	30	5	15.4
			24.4[18]	23	5.5	15.5
Chimera 7	15.2 ± 0.3	-2.0 ± 0.4	2.5	25	5.5	16.9
Chimera 4	15.0 ± 0.2	-0.8 ± 0.3	15.4	25	5.5	15.8
Chimera 3	15.8 ± 0.3	0.7 ± 0.4	1.8	25	6.0	17.1
Chimera 1	15.4 ± 0.3	0.3 ± 0.4	-	-	-	-
YopH WT	14.1 ± 0.2	-2.9 ± 0.3[1]	1235[19]	30	5	13.5
			601[20]	30	5.5	13.9
			750[15]	25	5.5	13.6

[a] All calculated values ($\Delta G^{\ddagger}_{calc}$ and $\Delta G_{0,calc}$) are averages and standard errors of the mean over 30 individual EVB trajectories per system, as described in the **Materials and Methods**. All energies are presented in kcal mol^{-1}. Shown here are also the corresponding experimental data, where available for each variants, specifically the kinetics (k, s^{-1}) and activation free energies ($\Delta G^{\ddagger}_{exp}$) derived from the experimentally observed rates using the Eyring equation. Note that, as described in the main text, Chimera 1 is not active, and is presented here only for comparison.

Table S8. Electrostatic contributions of individual amino acids ($\Delta\Delta G^{\ddagger}_{elec}$, kcal mol^{-1}) to the calculated activation free energies for the hydrolysis reaction catalyzed by WT PTP1B and relevant chimeras. These results are presented graphically in **Figure S12**.

Amino Acid	WT PTP1B	Chimera 7	Chimera 4	Chimera 3	Chimera 1
R24	0.06 ± 0.00	0.08 ± 0.01	0.09 ± 0.00	0.19 ± 0.01	0.17 ± 0.01
R45	-0.05 ± 0.01	-0.06 ± 0.00	-0.11 ± 0.00	-0.13 ± 0.01	-0.15 ± 0.00
T84	0.16 ± 0.00	0.15 ± 0.00	0.16 ± 0.00	0.15 ± 0.00	0.15 ± 0.00
L110	-0.16 ± 0.01	-0.17 ± 0.01	-0.18 ± 0.00	-0.18 ± 0.00	-0.18 ± 0.00
N111	0.21 ± 0.02	0.21 ± 0.02	0.22 ± 0.00	0.17 ± 0.01	0.18 ± 0.01
R112	0.40 ± 0.03	0.55 ± 0.05	0.29 ± 0.02	0.13 ± 0.01	0.13 ± 0.02
E115	-0.92 ± 0.02	-0.89 ± 0.03	-0.71 ± 0.03	-0.34 ± 0.03	-0.41 ± 0.03
K116	0.56 ± 0.05	0.44 ± 0.04	0.53 ± 0.05	0.84 ± 0.06	0.77 ± 0.05
K120	2.37 ± 0.14	2.12 ± 0.15	1.61 ± 0.10	1.06 ± 0.03	1.12 ± 0.04
R156	-0.16 ± 0.00	-0.16 ± 0.00	-0.16 ± 0.0	-0.18 ± 0.00	-0.18 ± 0.00
F182Qb	0.23 ± 0.01	0.58 ± 0.02	0.55 ± 0.02	0.91 ± 0.02	0.91 ± 0.02
H214	-0.19 ± 0.00	-0.18 ± 0.00	-0.21 ± 0.00	-0.19 ± 0.00	-0.19 ± 0.00
S216	-0.67 ± 0.04	-0.59 ± 0.03	-0.49 ± 0.03	-0.55 ± 0.03	-0.61 ± 0.02
A217	-0.19 ± 0.00	-0.17 ± 0.00	-0.20 ± 0.00	-0.17 ± 0.00	-0.16 ± 0.00
G218	-0.56 ± 0.00	-0.55 ± 0.00	-0.58 ± 0.00	-0.54 ± 0.00	-0.53 ± 0.00
I219	-0.20 ± 0.00	-0.20 ± 0.00	-0.20 ± 0.00	-0.17 ± 0.00	-0.18 ± 0.00
G220	-0.17 ± 0.00	-0.14 ± 0.00	-0.17 ± 0.00	-0.11 ± 0.00	-0.11 ± 0.00
R221	-0.64 ± 0.02	-0.63 ± 0.02	-0.69 ± 0.02	-0.96 ± 0.02	-0.90 ± 0.02
S222	-0.81 ± 0.01	-0.82 ± 0.01	-0.85 ± 0.01	-0.83 ± 0.00	-0.82 ± 0.01
D229	0.24 ± 0.00	0.24 ± 0.00	0.24 ± 0.00	0.25 ± 0.00	0.23 ± 0.00
R254	-0.15 ± 0.00	-0.15 ± 0.00	-0.14 ± 0.00	-0.07 ± 0.00	-0.08 ± 0.00
R257	-0.69 ± 0.00	-0.67 ± 0.01	-0.70 ± 0.00	-0.65 ± 0.00	-0.64 ± 0.00
Q262	0.46 ± 0.05	0.01 ± 0.01	0.57 ± 0.04	0.18 ± 0.04	0.12 ± 0.03
D265	-0.13 ± 0.00	-0.14 ± 0.00	-0.15 ± 0.00	-0.19 ± 0.00	-0.19 ± 0.00

[a] Data was obtained from our calculated EVB trajectories using the linear response approximation (LRA)[21, 22] and is presented as average values and standard error of the mean over 30 individual trajectories per system. All electrostatic contributions were scaled assuming an internal dielectric constant of 4. [b] All chimeras carry the F182Q substitution.

Table S9. Calculated distances at the Intermediate states (IS), transition states (TS) and product states (PS) obtained from our EVB simulations.[a]

		S_{Cys}-P	P-O_{H2O}	O_{H2O}-H	H-O_{Asp}
PTP1B	**IS**	1.97 ± 0.01	3.17 ± 0.06	0.99 ± 0.01	2.06 ± 0.19
	TS	2.32 ± 0.02	2.11 ± 0.02	1.08 ± 0.01	1.25 ± 0.01
	PS	3.32 ± 0.03	1.61 ± 0.01	1.34 ± 0.02	1.01 ± 0.01
Chimera 7	**IS**	1.97 ± 0.01	3.50 ± 0.11	0.99 ± 0.01	2.45 ± 0.19
	TS	2.34 ± 0.02	2.14 ± 0.02	1.08 ± 0.01	1.25 ± 0.01
	PS	3.46 ± 0.04	1.60 ± 0.01	1.34 ± 0.01	1.00 ± 0.01
Chimera 4	**IS**	1.97 ± 0.01	3.03 ± 0.03	0.99 ± 0.01	1.79 ± 0.14
	TS	2.37 ± 0.02	2.04 ± 0.02	1.09 ± 0.01	1.23 ± 0.01
	PS	3.36 ± 0.04	1.61 ± 0.01	1.33 ± 0.01	1.01 ± 0.01
Chimera 3	**IS**	1.97 ± 0.01	3.12 ± 0.03	0.99 ± 0.01	3.49 ± 0.10
	TS	2.34 ± 0.02	2.10 ± 0.02	1.07 ± 0.01	1.25 ± 0.01
	PS	3.29 ± 0.03	1.61 ± 0.01	1.32 ± 0.01	1.01 ± 0.01
Chimera 1	**IS**	1.97 ± 0.01	3.13 ± 0.03	0.99 ± 0.01	3.45 ± 0.08
	TS	2.34 ± 0.02	2.10 ± 0.02	1.07 ± 0.01	1.25 ± 0.01
	PS	3.31 ± 0.03	1.61 ± 0.01	1.31 ± 0.01	1.01 ± 0.01
YopH	**IS**	1.97 ± 0.01	3.18 ± 0.03	0.99 ± 0.01	2.33 ± 0.19
	TS	2.33 ± 0.02	2.12 ± 0.02	1.08 ± 0.01	1.24 ± 0.01
	PS	3.28 ± 0.03	1.62 ± 0.01	1.34 ± 0.01	1.01 ± 0.01

[a] IS, TS and PS correspond to the phosphoenzyme intermediate, transition state for the hydrolysis step and product state, respectively (**Figure 1**). S_{Cys-P} denotes the distance between the cysteine side chain and the phosphorus atom of the phosphate group, P-O_{H2O} denotes the distance between the phosphorus atom and the nucleophilic water molecule in the hydrolysis step, O_{H2O}-H denotes the distance between the nucleophilic water molecule and the proton being transferred back to the aspartic acid side chain, and H-O_{Asp} denotes the distance between the proton and the relevant oxygen atom of the aspartic acid side chain. All distances are shown in Å. Data is presented as average values and standard error of the mean over 30 individual EVB trajectories per system.

Supplementary References

1. R. M. Crean, M. Biler, M. W. van der Kamp, A. C. Hengge and S. C. L. Kamerlin, *J. Am. Chem. Soc.*, 2021, **143**, 3830-3845.
2. V. B. Chen, W. B. Arendall, 3rd, J. J. Headd, D. A. Keedy, R. M. Immormino, G. J. Kapral, L. W. Murray, J. S. Richardson and D. C. Richardson, *Acta Crystallogr. D:*, 2010, **66**, 12-21.
3. C. R. Sondergaard, M. H. Olsson, M. Rostkowski and J. H. Jensen, *J. Chem. Theory Comput.*, 2011, **7**, 2284-2295.
4. D. A. Keedy, Z. B. Hill, J. T. Biel, E. Kang, T. J. Rettenmaier, J. Brandão-Neto, N. M. Pearce, F. von Delft, J. A. Wells and J. S. Fraser, *eLife*, 2018, **7**, 1-36.
5. R. Shen, R. M. Crean, S. J. Johnson, S. C. L. Kamerlin and A. C. Hengge, *JACS Au*, 2021, **1**, 646–659.
6. J.-P. Ryckaert, G. Ciccotti and H. J. C. Berendsen, *J. Comp. Phys.*, 1977, **23**, 327-341.
7. T. Darden, D. York and L. Pedersen, *J. Chem. Phys.*, 1993, **98**, 10089-10092.
8. M. J. Chen, J. E. Dixon and G. Manning, *Sci. Signal.*, 2017, **10**, eaag1796.
9. J. Phan, K. Lee, S. Cherry, J. E. Tropea, T. R. Burke, Jr. and D. S. Waugh, *Biochemistry*, 2003, **42**, 13113-13121.
10. A. G. Evdokimov, M. Pokross, R. Walter, M. Mekel, B. Cox, C. Y. Li, R. Bechard, F. Genbauffe, R. Andrews, C. Diven, B. Howard, V. Rastogi, J. Gray, M. Maier and K. G. Peters, *Acta Crystallogr., Sect D*, 2006, **62**, 1435-1445.
11. G. King and A. Warshel, *J. Chem. Phys.*, 1989, **91**, 3647-3661.
12. G. H. Peters, S. Branner, K. B. Moller, J. N. Andersen and N. P. Moller, *Biochimie*, 2003, **85**, 527-534.

13. Z.-Y. Zhang, W. P. Malochowski, R. L. Van Etten and J. E. Dixon, *J. Biol. Chem.*, 1994, **269**, 8140-8145.

14. D. S. Cui, J. M. Lipchock, D. Brookner and J. P. Loria, *J. Am. Chem. Soc.*, 2019, **141**, 12634-12647.

15. G. Moise, Y. Morales, V. Beaumont, T. Caradonna, J. P. Loria, S. J. Johnson and A. C. Hengge, *Biochemistry*, 2018, **57**, 5315-5326.

16. J. A. Stuckey, H. L. Schubert, E. B. Fauman, Z. Y. Zhang, J. E. Dixon and M. A. Saper, *Nature*, 1994, **370**, 571-575.

17. S. K. Whittier, A. C. Hengge and J. P. Loria, *Science*, 2013, **341**, 899-903.

18. T. A. S. Brandão, S. J. Johnson and A. C. Hengge, *Arch. Biochem. Biophys.*, 2012, **525**, 53-59.

19. Z. Y. Zhang, J. C. Clemens, H. L. Schubert, J. A. Stuckey, M. W. F. Fischer, D. M. Hume, M. A. Saper and J. E. Dixon, *J. Biol. Chem.*, 1992, **267**, 23759-23766.

20. Y. F. Keng, L. Wu and Z. Y. Zhang, *Eur. J. Biochem.*, 1999, **259**, 809-814.

21. F. S. Lee, Z. T. Chu, M. B. Bolger and A. Warshel, *Protein Eng.*, 1992, **5**, 215-228.

22. I. Muegge, H. Tao and A. Warshel, *Protein Eng.*, 1997, **10**, 1363-1372.